Research Article

iMedPub Journals
http://www.imedpub.com

Journal of Pediatric Care
ISSN 2471-805X

2015
Vol. 1 No. 1:2

DOI: 10.21767/2472-1123.100002

Synthesis and Characterization of a Flower-Structured Ferromagnetic Nickel Oxide Nanoparticle: Investigation of Photocatalytic Activity

Dhananjay Dey[1], Subrata Das[1], Moumita Patra[2], Niranjan Kole[1] and Bhaskar Biswas[1]

1 Department of Chemistry, Raghunathpur College, Purulia, West Bengal, India

2 Department of Physics, Raghunathpur College, Purulia, West Bengal, India

Corresponding author: Bhaskar Biswas

icbbiswas@gmail.com

Department of Chemistry, Raghunathpur College, Purulia-723 133, West Bengal, India.

Tel: +91 3251 255235
Fax: +91 3251 255235

Citation: Dey B, Das S, Patra M, et al. Synthesis and Characterization of a Flower-Structured Ferromagnetic Nickel Oxide Nanoparticle: Investigation of Photocatalytic Activity. J Org Inorg Chem. 2015, 1:1.

Abstract

Flower-structured nickel oxide nanoparticle (NiONP) with flower size ~ 400-700 nm and petel size (individual nanoparticle) ~ 100 diameter have been successfully fabricated via an optimized thermo-decomposition technique using a dinuclear nickel(II)-Schiff base precursor. The template-free method is facile and effective in preparing flower-shaped NiO superstructures in high yield. The NiONP is characterized by scanning electron microscopy (SEM), powder X-ray diffraction (PXRD), Fourier transform IR (FTIR), and optical absorption spectroscopy (UV-Vis). Magnetic study reveals that the existence of super-paramagnetic (weak ferromagnetic) phenomenon in the synthesized NiO nanoparticle. NiONP has been employed as photocatalytic agent to degrade the organic dye, viz., Rhodamin-B (RhB) under visible light and by exposing to visible light for 1 h, NiONP degraded RhB dye nearly 100%.

Keywords: NiO nanoparticle; SEM image; Magnetic measurement; Dye degradation

Received: August 24, 2015; **Accepted:** October 07, 2015; **Published:** October 14, 2015

Introduction

Nanoscale materials have been pursued extensively for their unique physical and chemical properties and promising applications in nano-devices compared to those of their bulk counterparts [1]. The morphology, crystallography and size of the nano-structured materials can greatly influence their optical, electronic, magnetic, and catalytic properties [2]. Among transition metal oxides, nickel oxide (NiO) bulk and nano size have received considerable attention due to their wide range of applications in different fields, such as: catalysis [3], fuel cell electrodes and gas sensors [4], electrochromic films [5], battery cathodes [6], magnetic materials [7], and photovoltaic devices [8]. Because of the quantum size and surface effects, NiO nanoparticles exhibit catalytic, optical, electronic, and magnetic properties that are significantly different than those of bulk-sized NiO particles [9]. In addition, nanostructured NiO, because of its large chemical and thermal stability, also shows great promise for the use in energy conversion applications. Further, combustion synthesis is a particularly simple, safe and rapid fabrication process wherein the main advantages are energy and time saving. This quick, straightforward process can be used for synthesis homogenous, high purity, crystalline oxide ceramic powders including ultra-fine nickel powders with a broad range of particle sizes. Excess apply of various dyes in the textile industry has led to the severe surface water and groundwater contamination by releasing the toxic and coloured effluents, which are usually disposed by various physical and chemical methods, such as coagulation/flocculation [10], electrocoagulation [11], coagulation/carbon adsorption process [12] and so on. However, these methods barely transfer the pollutants from one phase to another without destruction or have the other limitations. In this present work, we have synthesized and structurally characterized a dinuclear Ni(II)-Schiff base complex which has been used to synthesize NiONP of ~ 100 nm by pyrolytic technique. The nanoparticle has been characterized by different spectroscopic tools including powder X-ray diffraction study and scanning electron microscope imaging. Magnetic measurement reflects the existence of weak ferromagnetism

in NiONP. The visible light driven photocatalytic activity of synthesized NiO nanoparticle has been demonstrated using rhodamin B (RhB) as a representative dye and the catalytic efficiency is optimized with respect to pH of the solution.

Experimental

Preparation of the precursor

Chemicals, solvents and starting materials: High purity 2-aminophenol (E. Merck, India), *O*-vanilin (Lancaster, UK), rhodamin B (Aldrich, USA), nickel(II) acetate tetrahydrate (E. Merck, India) were purchased from respective concerns and used as received. All the other reagents and solvents are of Analytical grade (A.R. grade) and were purchased from commercial sources and used as received.

General synthesis of the Schiff base ligand (H_2L) and its nickel compound (1): The Schiff base ligand, H_2L, and its nickel(II) complex were synthesized using a previously reported literature by our group [13]. To prepare the Schiff base ligand, *O*-aminophenol (0.1092 g, 1 mmol) was refluxed with *O*-vanilin (0.1523 g, 1 mmol) in 20 ml dehydrated alcohol and red coloured crystalline compound was isolated from solution, which was dried and stored *in vaccuo* over $CaCl_2$ for subsequent use. Yield 0.213 g (87.2%). Anal cal. for $C_{14}H_{13}NO_3$ (H_2L): C, 69.12; H, 5.39; N, 5.76; Found: C, 69.03; H, 5.30; N, 5.68 IR (KBr pellet, cm^{-1}): 3365 (s) (ν_{OH}), 1618 (s), 1595 (s) ($\nu_{C=N}$), 1509 (s), 1462 (s), 1333 (s), 1245 (s) (ν_{OAr}); UV-Vis (λ_{max}, nm): 233, 275, 347, 461; ^{1}H NMR (δ ppm, 300 Mz, DMSO-d^6) δ=13.55 (s, 1H), 9.92 (s, 1H), 8.48 (s, 1H), 7.26-6.81 (Ar-H, 7H), 4.27 (t, 1H), 3.92 (s, 3H) ppm. A methanolic solution (5 cm^3) of H_2L (0.244 g, 1 mmol) was added dropwise to a solution of $Ni(OAc)_2.4H_2O$ (0.496 g, 2 mmol) in the same solvent (10 cm^3). The red solution of the ligand turned into brown and after filter the supernatant liquid was kept in air for slow evaporation.

Yield: 0.342 g (69% based on metal salt). Anal. Calc. for $C_{19}H_{25}NO_{10}Ni_2$ (**1**): C, 41.89; H, 4.63; N, 2.57. Found: C, 41.80; H, 4.57; N, 2.64%. IR (KBr, cm^{-1}): 3398 (ν_{OH}), 1621, 1605 ($\nu_{C=N}$), 1475, 1434 $(\nu_{OAc})_{sym}$; UV-Vis (λ_{max}, nm): 236, 310, 376, 424.

Physical measurements

Infrared spectrum (KBr) was recorded with a FTIR-8400S SHIMADZU spectrophotometer in the range 400–3600 cm^{-1}. ^{1}H NMR spectrum in DMSO-d_6 was obtained on a Bruker Avance 300 MHz spectrometer at 25°C and was recorded at 299.948 MHz. Chemical shifts are reported with reference to $SiMe_4$. Ground state absorption was measured with a JASCO V-730 UV-vis spectrophotometer. Thermal analysis was carried out on a PerkinElmer Diamond TG/DTA system up to 800°C in a static nitrogen atmosphere with a heating rate of 10°C/min. Elemental analyses were performed on a Perkin Elmer 2400 CHN microanalyser. The pH value of the solutions was measured by Systronics pH meter at room temperature.

Physicochemical characterization of NiOnanopartcle

Size and morphology of the 100 nm NiO nanoparticle was characterized by powder X-ray diffraction (PXRD) pattern and Scanning Electron Microscopy (SEM) to examine their structure, shape and surface morphology. The XRD pattern was measured by X-ray diffractometer (Bruker D8 advance) in the range from 30°-80° using CuK_α radiation. The SEM image has been obtained using a microscope (FESEM, JEOL, and JSM-6700F).

Photocatalytic experiments

The photocatalytic activity of NiO nanoparticle was evaluated by degradation of rhodamin-B (RhB) dye solution (**Scheme 2**). All the experiments were carried out in presence of visible light using a previously reported procedure by our group [14]. A 250 ml Borosil beaker with outside water circulation was placed on a magnetic stirrer, above which a high pressure mercury vapour lamp (125 W, Philips) emitting visible light was placed. NiO nanoparticle at a dose of 100 mg (solid) was added to 100 ml RhB dye solution (1.2×10^{-4} M) in the beaker at an ambient condition. The distance of the light source from the upper level of dye solution is 18 cm for maximum utilization of light. The solution was stirred in dark for 10 minutes to establish the adsorption equilibrium. The zero time reading was taken and the solution was then irradiated with visible light. Aliquots of 5 ml samples were taken at regular time interval (10 minutes) and centrifuged to analyse the percent degradation of the RhB dye. The percentage dye degradation was calculated using formula:

$$\text{Degradation}=[(A_o - A_t)/A_o] \times 100\%,$$

Where, A_o is the initial dye absorbance; A_t is the dye absorbance at time (t).

To study the effect of pH on degradation efficiency, the pH of the RhB dye solution was systematically adjusted by adding 0.1 M HCl or NaOH.

Results and Discussion

Synthesis of the NiO nanoparticle and its mechanistic aspects

The Schiff base ligand, H_2L, and its acetate-bridged dinuclear nickel(II) complex was prepared by mixing nickel(II) acetate and the ligand in methanol-water (95/5; v/v) medium. The coordination geometry of this nickel precursor and its structural formulation was determined by different spectroscopic and analytical techniques. The schematic presentation of syntheses is given below (**Scheme 1**). Thermal decomposition study of this dinuclear nickel(II) complex precursor is reported earlier [13]. Thermogram of the dinickel(II)-Schiff base complex show well distinct stepwise decomposition (**Figure S1**). On heating at 450°C for 4 h in a furnace, the precursor generates NiONP as thermally stable end product (expt. wt loss=77.90% at 399°C, theo. wt. loss=81.73%). The synthetic procedure to obtain the nanoparticle was optimized in varying the thermal decomposition temperature at 450 and 500°C. From the thermogram of the dinuclear nickel precursor (**Figure S2**), it was seen that below 400°C there was substantial existence of thedinuclear precursor. It was also observed that at 500°C the surface energy is not in a minimized state to form flower-structured NiO nano particle and as a result flower shaped.

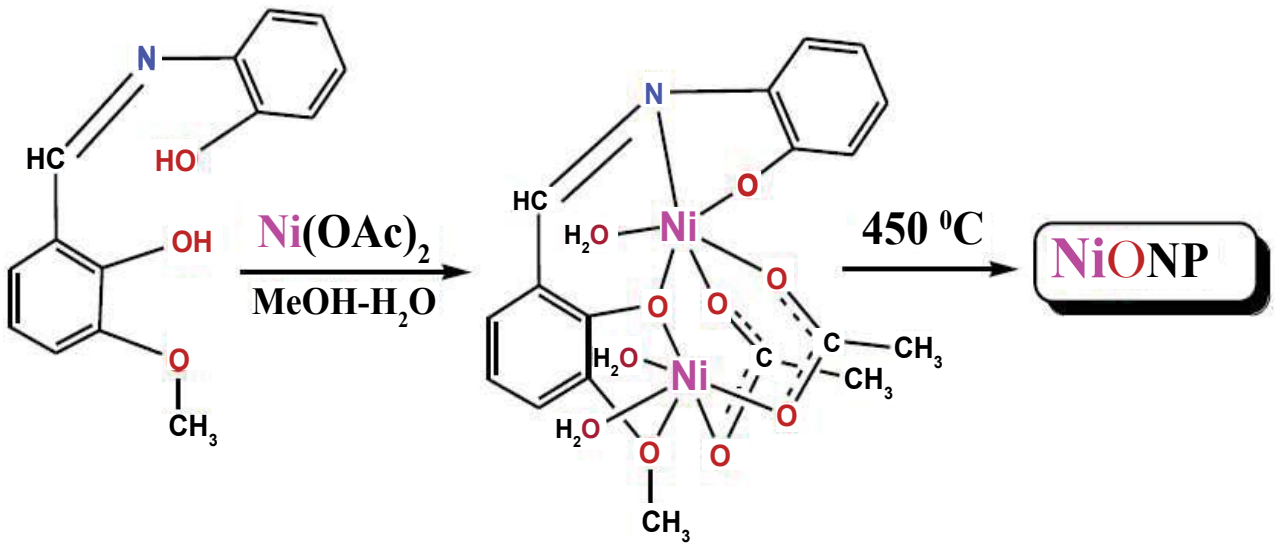

Scheme 1 Preparative procedure of the NiO nanoparticle.

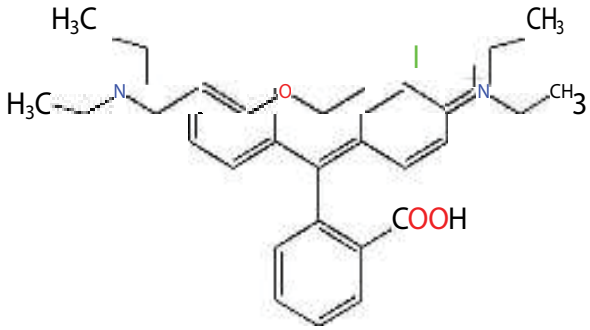

Scheme 2 Structure of rhodamin B dye.

Infrared spectroscopy analysis of metal oxide nano particles

FT-IR spectra of the thermally stable end product NiO is represented in (**Figure S3**). The spectrum show a strong band at 486 cm^{-1} which assigned to the Ni–O stretching of the octahedral NiO_6 groups in the face center cubic NiO structure [15]. At this temperature, no bands appeared at about 3550 and 1650 cm^{-1} which suggested that no water molecules absorbed by the sample or KBr during FTIR experiment.

XRD patterns of NiO nanoparticle

XRD patterns of NiO compound reflect that all the diffraction peaks of NiO match the standard data for a NiO nanoparticle. All the diffraction peaks (**Figure 1**) can be well indexed with the Fm3m space group (JCPDS file No. 07-0230). The sharp and intense peaks in **Figure 1** indicate that the samples are highly crystalline. The cubic lattice parameters obtained by CELSIZ programme of the nanoparticle is =4.17249.

Scanning electron microscopy image (SEM)

To obtain detailed information about the microstructure and morphology of the synthesized NiO nanoparticle, scanning electron microscopy (SEM) was carried out. **Figure 2** represents the image of pure NiO nanoparticle powders. It can be seen clearly that the powders are in flower shape of diameter ~ 400-700 nm. The individual grain size of the nanoparticle is ~ 100 nm.

V-Vis spectrum of NiONp

It is well known that the optical absorption behaviour of photo-catalyst could significantly affect the photocatalytic activity. For the characterization of the fabricated NiONPs, in the present study, an UV-Vis spectrophotometer was employed to record the absorbance spectrum in the wavelength range of 200 to 900 nm for dispersed NiONP in distilled water. The absorbance spectrum of NiONP is shown in **Figure S4**. A strong absorption band ranging from 200 to 450 nm was observed for NiONPs due to the metal ion [16]. The n→σ* absorption bands appeared at approximately 269 nm and the n→π* absorption band was observed at 324 nm. This UV-Vis spectrum is consisted with previously reported data [16]. The band gap energy of NiO nanoparticles was calculated based on the absorption spectrum of the NiONp according to the equation, $E_{bg}=1240/\lambda$ (eV),

where, E_{bg} is the band gap energy of the photocatalyst, λ is the wavelength in nm. The calculated band gap of the NiONp is 3.4 eV (**Figure S4**). This band gap value as 3.4 eV indicates that synthesized NiO has a suitable band gap for photocatalytic degradation of dyes.

Magnetic properties of NiONp

The magnetization versus magnetic field (M–H) curve of the flower structured NiO nanocrystalline sample is shown in **Figure**

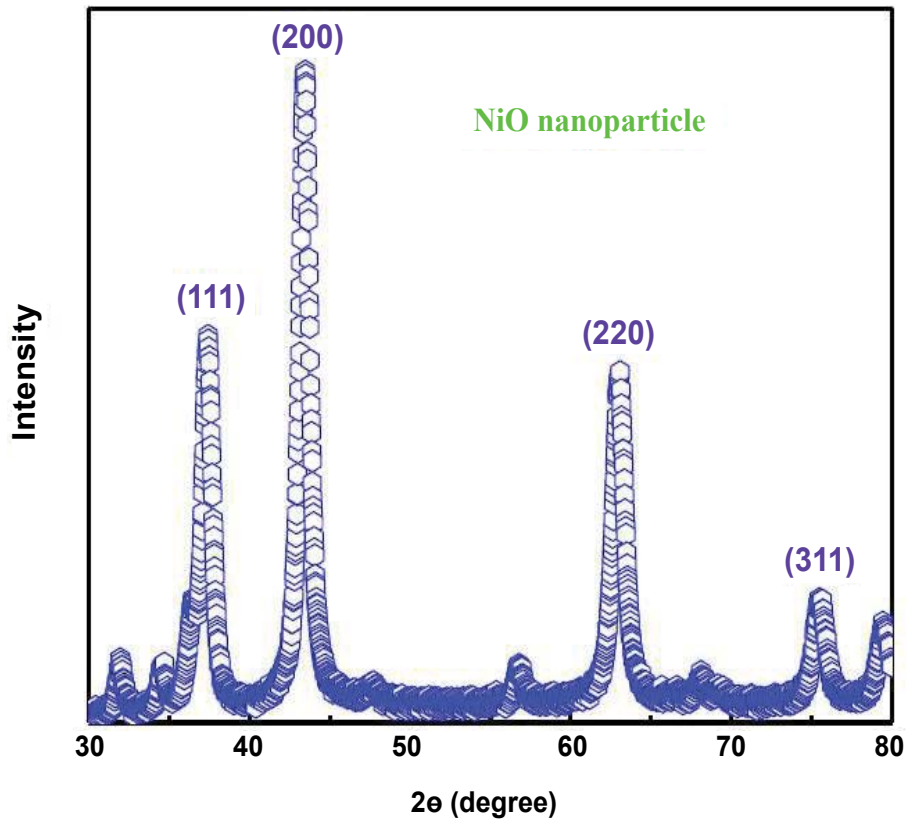

Figure 1 Structure of rhodamin B dye.

3. The NiO nanoparticles exhibit typical M–H behaviour at room temperature. **Figure 3** shows the isothermal magnetization for the NiOnps sample. The M–H curve reveals that at higher fields the magnetization increases with increasing magnetic field and shows no sign of saturation in the field range investigated up to 50 kOe. The obtained value of coercivity is 220 Oe for this sample. These behaviors indicate that the NiO nanocrystalline samples exhibit a ferromagnetic character in contrast to antiferromagnetic bulk material [17]. The appearance of weak ferromagnetic-like behaviour may probably due to the presence of superparamagnetic metallic Ni clusters or the Ni^{3+} ions within the NiO lattice [18,19]. However, no traces of metallic Ni cluster and Ni^{3+} ions and other ferromagnetic impurities are detected by XRPD. Therefore, the weak ferromagnetism observed originates from the NiO nanocrystallite system. The weak ferromagnetic-like behavior in our sample may be attributed to the broken bonds and lattice distortion [19-21]. It is well known that the lattice distortion usually occurs in the nano-scaled particles. However, further work is needed to achieve a thorough understanding of the origin of weak ferromagnetism for the nano-scaled antiferromagnetic particles.

Photocatalytic activity of NiONp under visible light

Rhodamin B is a heterocyclic aromatic chemical compound with the molecular formula $C_{28}H_{31}N_2O_3Cl$. The spectrum of the RhB solution (**Figure S5**) in aqueous medium shows characteristics peaks at 267, 352, 406 and 540 nm. The decrease in absorbance of the aqueous solution at 540 nm with visible light illumination in the NiONP suspension is due to the breakdown of the chromophore (**Figure 4**). The photodegradation of rhodamin B was employed to evaluate the photocatalytic activities of the NiO nanoparticles. The photocatalytic properties of NiONP are known to depend on several factors like size, morphology, surface area and electronic state. The self-degradation of RhB in visible light was negligible in the absence of photocatalyst. It is proved that when the particle sizes of nanostructures increase beyond the optimum size, the photocatalytic activity decreases due to decrease in surface area [22]. The NiONP synthesized by pyrolytic method took 60 min, for maximum RhB degradation.

Mechanistic pathway for photocatalytic degradation by nanoparticle

The photocatalytic degradation of a dye in the presence of metal oxide nanoparticle is initiated by photoexcitation of the nanoparticle which leads to the formation of electron-hole pair [16]. Part of these photogenerated carriers recombines RhB in the bulk of the nanoparticle, while the rest migrate to the surface of the catalyst, where the holes act as powerful oxidants and electrons as powerful reluctant. The high oxidative potential of the hole causes the direct oxidation of the dye to reactive intermediates [16]. In the other hand hydroxyl radicals are formed by the decomposition of water or by the reaction of hole with OH^-, behave as reactive intermediate for degradation. Probably,

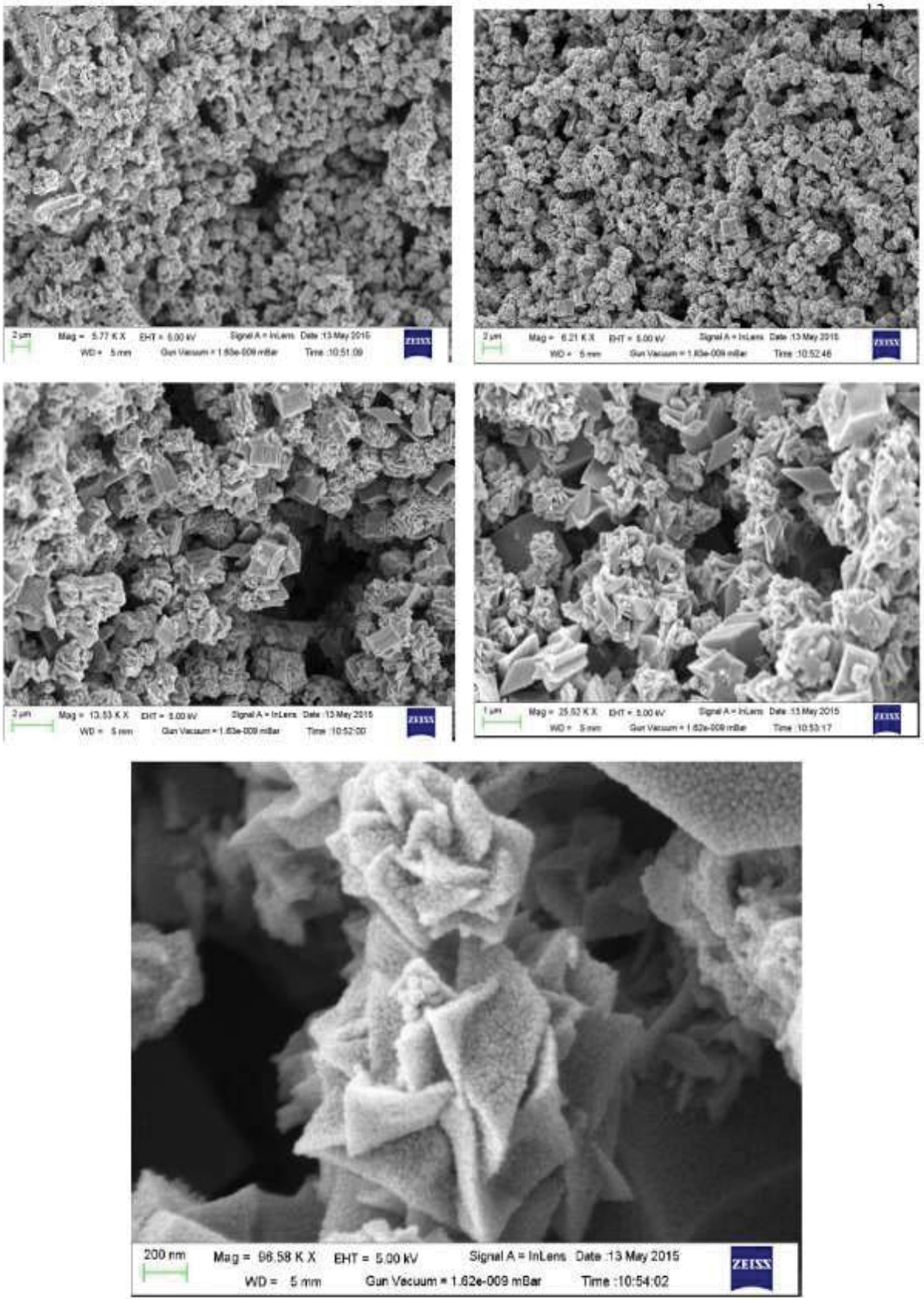

Figure 2 Series of SEM images in varying magnification range from 5.77 K X to 96.58 K, showing gradual formation of flower shaped NiO nanoparticles at 450°.

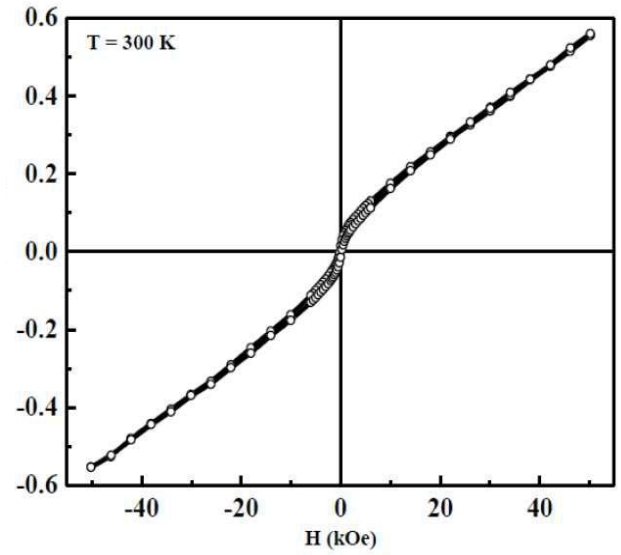

Figure 3 M-H plot of NiO nanoparticle.

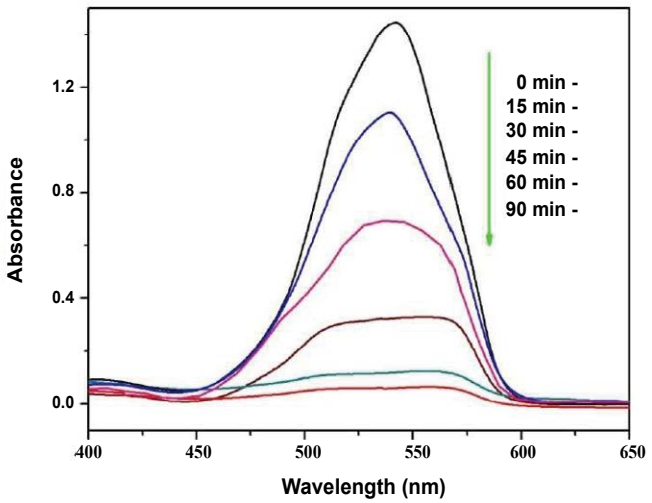

Figure 4 Adsorption changes of RhB aqueous solution at room temperature in the presence of NiO nanoparticles obtained under visible light radiation.

the hydroxyl radical is an extremely non-selective oxidant which leads to partial or complete mineralization of the dye.

i) NiO + h_{v} → e^- + h^+; ii) O_2 + e^- → $O_2^{\bullet-}$; iii) h^+ + H_2O → $OH^\bullet$ + H^+; iv) h^+ + OH^- → $OH^\bullet$; v) Dye + $OH^\bullet$ → RCOO$^\bullet$ → CO_2 + H_2O

Alternatively, the electron in the conduction band can be picked up by the adsorbed dye molecules, leading to the formation of the dye radical anion which is subsequently degraded.

In such photocatalytic process, the separation and recombination of photogenerated charge carriers are competitive pathways and photocatalytic activity is effective when recombination between them is prevented.

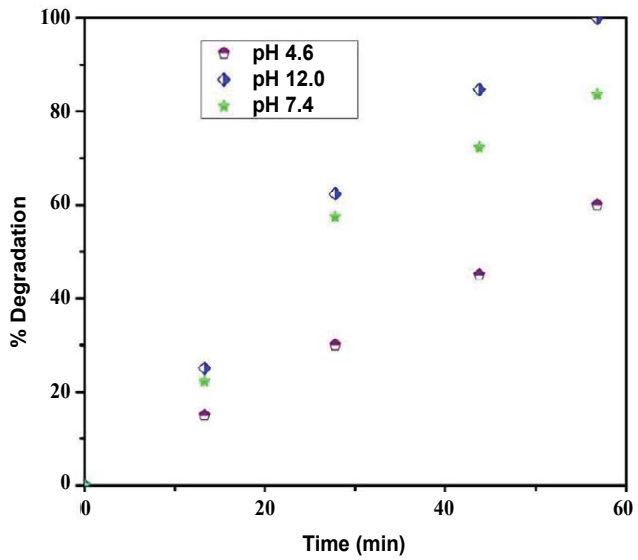

Figure 5 Changes of percentage degradation of RhB in aqueous solution at different pH in the presence of NiO nanoparticles under visible light irradiation at room temperature.

Effect of pH

The effect of pH on the photocatalytic activity was studied by varying the pH of the dye solution for 1 h. It can be seen from **Figure 5** that pH has a significant effect on the photodegradation rate. From the Figure it is seen that the rate of degradation is directly proportional to solution pH. At normal condition NiONp degraded 82.6% RhB dye at pH ~ 7.4 under visible light. When we increased the pH upto 12 for RhB in aqueous solution, the % degradation increases up to 99.9%, but with decrease in pH ~4.6 of the RhB, degradation percentage decreased in a greater extent (~60%). It can be rationalized with the fact that there exists an electrostatic interaction between the catalyst surface and the dye molecules which consequently enhances or inhibits the photodegradation rate [23]. The effect of pH value on photocatalysis is generally due to surface charge of the catalyst and the charge on dye molecules [24]. The change in pH shifts the redox potentials of the valence and conduction bands, which might affect the interfacial charge transfer [25]. The surface of NiO is positively charged at low pH whereas with rise in pH the surface becomes negatively charged. As RhB is a cationic dye, high pH favours the adsorption of dye molecule on the catalyst surface which results in high degradation efficiency. The degradation rate was found to be enhanced in alkaline conditions and maximum activity was obtained at pH 12. At pH 12, 99.9% dye degradation is observed for NiONP (**Figure 5**).

Conclusions

Herein we report the synthesis and structural characterization of a highly ordered flower-shaped NiONP super structure in high yield using a template-free facile and effective method. Magnetic study reveals the existence of super-paramagnetic (weak ferromagnetic) phenomenon in the synthesized NiO

nanoparticle. NiONP has been employed as photocatalytic agent to degrade the organic dye, viz. Rhodamin-B (RhB) under visible light and by exposing to visible light for 1 h, NiONP degraded RhB dye nearly 100%. In the presence of visible light, NiONP can efficiently catalyze the decolorization and degradation of RhB in the aqueous suspension. Photodegradation of RhB is accelerated by the increase of pH of its solution in the range of 4.6 to 12. The prepared NiONP has been found to be quite stable under visible light illumination at a pH of approximately 7.4, and there is some activation of the surfaces of NiO particles by this light.

Acknowledgements

The work is supported financially by the Department of Science and Technology (DST), New Delhi, India under FAST TRACK SCHEME for YOUNG SCIENTIST (NO. SB/FT/CS-088/2013 Dt. 21/05/2014). BB gratefully acknowledges Prof. T Pal, IIT Kharagpur for recording SEM image of the NiONP. BB is highly thankful to IACS, Kolkata for providing proton NMR, mass spectroscopy, PXRD and studies.

References

1 Rueckes T, Kim K, Joselevich E, Tseng GY, Cheung CL, et al. (2000) Carbon nano tube based non-volatile random access memory for molecular computing. Science 289: 94-97.

2 Cui Y, Lieber CM (2001) Functional nanoscale electronic devices assembled using silicon nanowire building blocks. Science 29: 851-853.

3 Nagi RE, Radwan MS, El-Shall M, Hassan MA (2007) Synthesis and characterization of nanoparticle Co_3O_4, CuO and NiO catalysts prepared by physical and chemical methods to minimize air pollution. Appl Catal A Gen 331: 8-18.

4 Hotovy I, Huran J, Spiess L, Hascik S, Rehacek V (1999) Preparation of nickel oxide thin films for gas sensors applications. Sens. Actuators B Chem 57: 147-152.

5 Miller EL, Rocheleau RE (1997) Electrochemical behavior of reactively sputtered iron-doped nickel oxide. J Electrochem Soc 144: 3072-30775.

6 Zhang FB, Zhou YK, Li HL (2004) Nanocrystalline NiO as an electrode material for electrochemical capacitor. Mater Chem Phys 83: 260-264.

7 Proenca MP, Sousa CT, Pereira AM, Tavares PB, Ventura J, et al. (2011) Size and surface effects on the magnetic properties of NiO nanoparticles. Phys Chem Chem Phys 13: 9561-9567.

8 Nathan T, Aziz A, Noor AF, Prabaharan SR (2008) Nanostructured NiO for electrochemical capacitors: Synthesis and electrochemical properties. J Solid State Electrochem 12: 1003-1009.

9 Schmidt G (2004) Nanoparticles: From Theory to Application. VCH: Weinheim, Germany.

10 Ghosh M, Biswas K, Sundaresan A, Rao CNR (2006) MnO and NiO nanoparticles: Synthesis and magnetic properties. J Mater Chem 16: 106-111.

11 He J, Lindstroem H, Hagfeldt A, Lindquist SE (1999) Dye-sensitized nanostructured p-type nickel oxide film as a photocathode for a solar cell. J Phys Chem B 103: 8940-8943.

12 Tao F, Shen Y, Wang L (2012) Controlled Fabrication of Flower-like Nickel Oxide Hierarchical Structures and Their Application in Water Treatment. Molecules 17: 703-715.

13 Dey D, Pal S, Chandraleka S, Dhanasekaran D, Kole N, et al. (2014) Synthesis and spectroscopic characterization of a dinuclear nickel complex: A bio-relevant catalyst and its reactivity. Journal of Indian Chemical Society 91: 1267-1276.

14 Dey D, Kaur G, Patra M, Choudhury AR, Kole N, et al. (2014) A perfectly linear trinuclear zinc-Schiff base complex: Synthesis, luminescence property and photocatalytic activity of zinc oxide nanoparticle. Inorg Chim Acta 421: 335-341.

15 Borgstrom M, Blart E, Boschloo G, Mukhtar E, Hagfeldt A, et al. (2005) Sensitized hole injection of phosphorus porphyrin into NiO: Toward new photovoltaic devices. J Phys Chem B 109: 22928-22934.

16 Deraz NM, Selim MM, Ramadan M (2009) Processing and properties of nanocrystalline Ni and NiO catalysts. Mater Chem Phys 113: 269-275.

17 Chantrell RW, El-Hilo M, O'Grady K (1991) A model of interaction effects in granular magnetic solids, IEEE Trans Magn 27: 3570-3578.

18 Richardson JT, Yiagas DI, Turk B, Forster K, Twigg MV, et al. (1991) Size-controlled nickel oxide nanoparticle synthesis using mesoporous silicon thin films. J Appl Phys 70: 6977-6982.

19 Bi H, Li S, Zhang Y, Du Y (2004) J Magn Magn Mater 277: 363-367.

20 Khadar A M., Biju V, Inoue A (2003) Effect of finite size on the magnetization behavior of nanostructured nickel oxide. Mater Res Bull 38: 1341-1349.

21 Seehra MS, Shim H, Dutta P, Manivannan A (2005) Interparticle interaction effects in the magnetic properties of NiO nanorods. J Appl Phys 97: 10J509.

22 Wei W, Jiang X, Lu L, Yang X, Wang X, et al. (2009) Study on the catalytic effect of NiO nanoparticles on the thermal decomposition of TEGDN/NC propellant. J Hazard Mater 168: 838-842.

23 Christy AJ, Umadevi M (2013) Novel combustion method to prepare octahedral NiO nanoparticles and its photocatalytic activity. Materials Res Bull 48: 4248-4254.

24 Zhao B, Ke XK, Bao JH, Wang CL, Dong L, et al. (2009) Synthesis of flower-like NiO and effects of morphology on its catalytic properties. J Phys Chem C 113: 14440-14447.

25 Park J, Kang E, Son SU, Park HM, Lee MK, et al. (2005) Monodisperse nanoparticles of Ni and NiO: Synthesis, characterization, self-assembled superlattices, and catalytic applications in the Suzuki coupling reaction. Adv Mater Weinheim 17: 429-434.